High-Fidelity Controlled- Z Gate with Maximal Intermediate Leakage Operating at the Speed Limit in a Superconducting Quantum Processor

Negîrneac, V.; Ali, H.; Muthusubramanian, N.; Battistel, F.; Sagastizabal, R.; Moreira, M. S.; Marques, J. F.; Vlothuizen, W. J.; Beekman, M.; Zachariadis, C.

DOI
10.1103/PhysRevLett.126.220502

Publication date
2021

Document Version
Final published version

Published in
Physical Review Letters

High-Fidelity Controlled-Z Gate with Maximal Intermediate Leakage Operating at the Speed Limit in a Superconducting Quantum Processor

V. Negîrneac,[1,2,*] H. Ali,[1,3,*] N. Muthusubramanian,[1,3] F. Battistel,[1] R. Sagastizabal,[1,3] M. S. Moreira,[1,3] J. F. Marques,[1,3] W. J. Vlothuizen,[1,4] M. Beekman,[1,4] C. Zachariadis,[1,3] N. Haider,[1,4] A. Bruno,[1,3] and L. DiCarlo[1,3]

[1]*QuTech, Delft University of Technology, P.O. Box 5046, 2600 GA Delft, Netherlands*
[2]*Instituto Superior Técnico, Universidade de Lisboa, 1049-001 Lisbon, Portugal*
[3]*Kavli Institute of Nanoscience, Delft University of Technology, P.O. Box 5046, 2600 GA Delft, Netherlands*
[4]*Netherlands Organisation for Applied Scientific Research (TNO), P.O. Box 96864, 2509 JG The Hague, Netherlands*

(Received 3 September 2020; accepted 6 April 2021; published 4 June 2021)

Simple tuneup of fast two-qubit gates is essential for the scaling of quantum processors. We introduce the sudden variant (SNZ) of the net zero scheme realizing controlled-Z (CZ) gates by flux control of transmon frequency. SNZ CZ gates realized in a multitransmon processor operate at the speed limit of transverse coupling between computational and noncomputational states by maximizing intermediate leakage. Beyond speed, the key advantage of SNZ is tuneup simplicity, owing to the regular structure of conditional phase and leakage as a function of two control parameters. SNZ is compatible with scalable schemes for quantum error correction and adaptable to generalized conditional-phase gates useful in intermediate-scale applications.

DOI: 10.1103/PhysRevLett.126.220502

Superconducting quantum processors have recently reached important milestones [1], notably the demonstration of quantum supremacy on a 53-transmon processor [2]. On the path to quantum error correction (QEC) and fault tolerance [3], recent experiments have used repetitive parity measurements to stabilize two-qubit entanglement [4,5] and to perform surface-code quantum error detection in a 7-transmon processor [6]. These developments have relied on two-qubit controlled-phase (CPhase) gates realized by dynamical flux control of transmon frequency, harnessing the transverse coupling J_2 between a computational state $|11\rangle$ and a noncomputational state such as $|02\rangle$ [7,8]. Compared to other implementations, e.g., cross resonance using microwave-frequency pulses [9] and parametric radio-frequency pulsing [10], baseband flux pulses achieve the fastest controlled-Z (CZ) gates (a special case of CPhase), operating near the speed limit $t_{\mathrm{lim}} = \pi/J_2$ [11].

Over the last decade, baseband flux pulsing for two-qubit gating has evolved in an effort to increase gate fidelity and to reduce leakage and residual ZZ coupling. In particular, leakage became a main focus for its negative impact on QEC, adding complexity to error-decoder design [12] and requiring hardware and operational overhead to seep [13–17]. To reduce leakage from linear-dynamical distortion in flux-control lines and limited time resolution in arbitrary waveform generators (AWGs), unipolar square pulses [8,18] have been superseded by softened counterparts [19,20] based on fast-adiabatic theory [21]. In parallel, coupling strengths have reduced to $J_2/2\pi \sim$ 10–20 MHz to mitigate residual ZZ coupling, which affects single-qubit gates and idling at bias points, and produces crosstalk from spectator qubits [22]. Many groups are actively developing tunable coupling schemes to suppress residual coupling without incurring slowdown [23–27].

A main limitation to the fidelity of flux-based CPhase gates is dephasing from flux noise, as one qubit is displaced 0.5–1 GHz below its flux-symmetry point (i.e., sweet spot [28]) to reach the $|11\rangle$–$|02\rangle$ resonance. To address this limitation, Ref. [29] introduced a bipolar variant [termed net zero (NZ)] of the fast-adiabatic scheme, which provides a built-in echo reducing the impact of low-frequency flux noise. The double use of the transverse interaction also reduces leakage by destructive interference, as understood by analogy to a Mach-Zehnder interferometer (MZI). Finally, the zero-average characteristic avoids the buildup of long-timescale distortions in the flux-control lines, significantly improving gate repeatability. NZ pulsing has been successfully used in several recent experiments [4,6,30], elevating the state of the art for CZ gate fidelity to $99.72 \pm 0.35\%$ [1]. However, NZ suffers from complicated tuneup, owing to the complex dependence of conditional phase and leakage on fast-adiabatic pulse parameters. This limits the use of NZ for two-qubit gating as processors grow in qubit count.

In this Letter, we introduce the sudden variant (SNZ) of the NZ scheme implementing CZ, which offers two advantages while preserving the built-in echo, destructive leakage interference, and repeatability characteristic of conventional NZ (CNZ). First, SNZ operates at the speed limit of transverse coupling by maximizing intermediate leakage to the non-computational state. The second and

main advantage is greatly simplified tuneup: the landscapes of conditional phase and leakage as a function of two pulse parameters have regular structure and interrelation, easily understood by exact analogy to the MZI. We realize SNZ CZ gates among four pairs of nearest neighbors in a seven-transmon processor and characterize their performance using two-qubit interleaved randomized benchmarking (2QIRB) with modifications to quantify leakage [29,31,32]. The highest performance achieved from one 2QIRB characterization has $99.93 \pm 0.24\%$ fidelity and $0.10 \pm 0.02\%$ leakage. SNZ CZ gates are fully compatible with scalable approaches to QEC [33]. The generalization of SNZ to arbitrary CPhase gates is straightforward and useful for optimization [34], quantum simulation [35], and other noisy intermediate-scale quantum (NISQ) applications [36].

A flux pulse to the $|11\rangle$–$|02\rangle$ interaction implements the unitary

$$U_{\mathrm{CPhase}} = \begin{pmatrix} 1 & 0 & 0 & 0 & 0 \\ 0 & e^{i\phi_{01}} & 0 & 0 & 0 \\ 0 & 0 & e^{i\phi_{10}} & 0 & 0 \\ 0 & 0 & 0 & \sqrt{1-4L_1}e^{i\phi_{11}} & \sqrt{4L_1}e^{i\phi_{02,11}} \\ 0 & 0 & 0 & \sqrt{4L_1}e^{i\phi_{11,02}} & \sqrt{1-4L_1}e^{i\phi_{02}} \end{pmatrix}$$

in the $\{|00\rangle, |01\rangle, |10\rangle, |11\rangle, |02\rangle\}$ subspace, neglecting decoherence and residual interaction between far off-resonant levels. Here, ϕ_{01} and ϕ_{10} are the single-qubit phases, $\phi_{11} = \phi_{01} + \phi_{10} + \phi_{2Q}$, where ϕ_{2Q} is the conditional phase, and L_1 is the leakage, The ideal CZ gate simultaneously achieves $\phi_{01} = \phi_{10} = 0(\mathrm{\ mod\ } 2\pi)$, $\phi_{2Q} = \pi(\mathrm{\ mod\ } 2\pi)$ (phase condition PC), and $L_1 = 0$ (leakage condition LC), with arbitrary ϕ_{02}.

The SNZ CZ gate is realized with two square half pulses with equal and opposite amplitude $\pm A$ and duration $t_p/2$ each. To understand its action, consider first the ideal scenario with perfectly square half pulses (infinite bandwidth), infinite time resolution, $t_p = t_{\mathrm{lim}}$, and $A = 1$ (corresponding to $|11\rangle$ and $|02\rangle$ on resonance). The unitary action of each complete half pulse (rising edge, steady level, and falling edge combined) implements one of two beam splitters in the MZI analogy: BS1 fully transmits $|11\rangle$ to $-i|02\rangle$ (producing maximal intermediate leakage), and BS2 fully transmits $-i|02\rangle$ to $-|11\rangle$, yielding an ideal CZ gate. SNZ adds an idling period t_ϕ between the half pulses to perfect the analogy to the MZI, allowing accrual of relative phase ϕ between $|02\rangle$ and $|11\rangle$ in between the beam splitters.

The key advantage of SNZ over CNZ is the straightforward procedure to simultaneously meet PC and LC. To appreciate this, consider the landscapes of ϕ_{2Q} and L_1 as a function of A and t_ϕ [Figs. 1(c) and 1(d)] in this ideal scenario. The landscapes have a clear structure and link to each other. The L_1 landscape shows a vertical leakage valley at $A = 1$ arising from perfect transmission at each beam splitter (LC1), and also two vertical valleys arising from perfect reflection (LC2). Leakage interference gives rise to additional diagonal valleys (LC3). Crucially, juxtaposing the $\phi_{2Q} = 180°$ contour shows that PC is met periodically, at the crossing of LC1 and LC3 valleys, where $\Delta_{02}^{\mathrm{max}} t_\phi = 0(\mathrm{\ mod\ } 2\pi)$ ($\Delta_{02}^{\mathrm{max}}$ is the detuning between $|02\rangle$ and $|11\rangle$ at the bias point). This regular leakage landscape therefore provides useful crosshairs for simultaneously achieving PC and LC. We note that $\phi_{2Q}(t_\phi)$ changes monotonically along the LC1 valley, allowing for CPhase gates with arbitrary ϕ_{2Q}. We leave this generalization for future work.

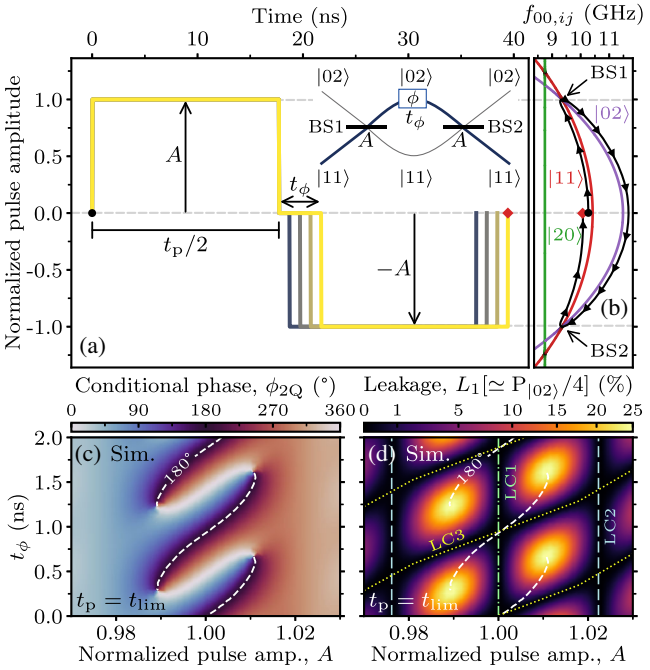

FIG. 1. Numerical simulation of an ideal SNZ pulse (infinite bandwidth and time resolution) using parameters for pair Q_L-Q_{M2} (see Table I). (a) Schematic of the ideal SNZ flux pulse, with $t_p = t_{\mathrm{lim}}$ and variable A and t_ϕ. The amplitude A is normalized to the $|11\rangle$–$|02\rangle$ resonance. Inset: MZI analogy for $A = 1$. (b) Transition frequency from $|00\rangle$ to levels $|ij\rangle$ in the two-excitation manifold as a function of instantaneous pulse amplitude. (c),(d) Landscapes of conditional phase ϕ_{2Q} (b) and leakage L_1 (c) as a function of A and t_ϕ.

There are practical reasons to include t_ϕ in experiment: any flux-pulse distortion remaining from the first half pulse (e.g., due to finite pulse decay time) will break the symmetry between BS1 and BS2. Because of the time resolution t_s of the AWG used for flux control, ϕ can only increment in steps of $-\Delta_{02}^{\mathrm{max}} t_s$. Typically $\Delta_{02}^{\mathrm{max}}/2\pi = 0.5$–$1$ GHz and $t_s \sim 1$ ns, so the number of intermediate sampling points only provides coarse control. For fine control, we propose to use the amplitude $\pm B$ of the first and last sampling points during t_ϕ [37].

We now turn to the experimental realization of SNZ CZ gates between nearest-neighbor pairs among four transmons. High- and low-frequency transmons (Q_H and Q_L, respectively) connect to two mid-frequency transmons (Q_{M1} and Q_{M2}) using bus resonators dedicated to each pair [connectivity diagram shown in Fig. 4(a) inset]. Each transmon has a flux-control line for two-qubit gating, a microwave-drive line for single-qubit gating, and dedicated readout resonators [4,38] (see Supplemental Material [37] for details). Each transmon is statically flux biased at its sweet spot to counter residual offsets. Flux pulsing is performed using a Zurich Instruments HDAWG-8 ($t_s = 1/2.4$ ns). Following prior work [29,44], we compensate the bandwidth-limiting effect of attenuation in the flux-control coaxial line (skin effect) and cryogenic reflective and absorptive low-pass filters using real-time digital filters in the AWG. In this way, we produce on-chip flux waveforms with rise time t_{rise} on par with that of the AWG (0.5 ns).

We exemplify the tuneup of SNZ using pair Q_L-Q_{M2} (Fig. 2). We first identify t_{lim} for the $|11\rangle$–$|02\rangle$ interaction and amplitude A bringing the two levels on resonance. Both

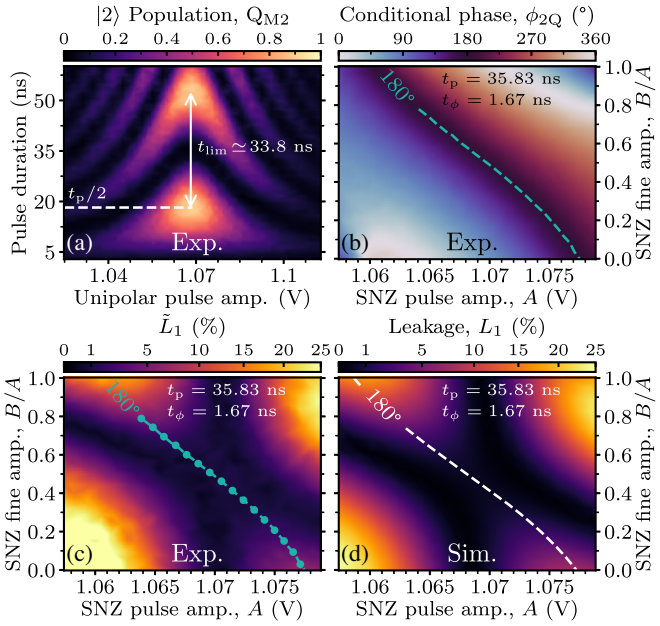

FIG. 2. Calibration of the SNZ pulse for pair Q_L-Q_{M2} and comparison to simulation. (a) $|2\rangle$-state population of Q_{M2} as a function of the amplitude and duration of a unipolar square pulse making $|11\rangle$ interact with $|02\rangle$. (b),(c) Landscapes of conditional phase ϕ_{2Q} and leakage estimate $\tilde{L}_1$ as a function of SNZ pulse amplitudes A and B, with $t_\phi = 1.67$ ns. The juxtaposed $\phi_{2Q} = 180°$ contour runs along the opposite diagonal compared to Figs. 1(b), 1(c) because increasing B (which decreases Δ_{02}) changes ϕ in the opposite direction from t_ϕ. Data points marked with dots are measured with extra averaging for examination in Fig. 3. (d) Numerical simulation of leakage L_1 landscape and $\phi_{2Q} = 180°$ contour with parameters and flux-pulse distortions from experiment. All landscapes (also in Fig. 3) are sampled using an adaptive algorithm based on [39].

are extracted from the characteristic chevron pattern of $|2\rangle$-population $P_{|2\rangle}$ in Q_{M2} as a function of the amplitude and duration of a unipolar square flux pulse acting on $|11\rangle$ [Fig. 2(a)]. The symmetry axis corresponds to $A = 1$. The difference in consecutive pulse durations achieving $P_{|2\rangle}$ maxima along this axis gives an accurate estimate of t_{lim} unaffected by initial transients. We set $t_p \equiv 2nt_s$, where n is the number of sampling points achieving the first $P_{|2\rangle}$ maximum. Using the measured positive difference $t_p - t_{\text{lim}}$ and numerical simulation (data not shown), we estimate $t_{\text{rise}} \approx 0.5$ ns. Next, we use standard conditional-oscillation experiments [29] to measure the landscapes of ϕ_{2Q} and leakage estimate $\tilde{L}_1$ for SNZ pulses over amplitude ranges $A \in [0.9, 1.1]$ and $B \in [0, A]$, keeping $t_\phi \gtrsim 3t_{\text{rise}}$. As expected, the landscape of $\tilde{L}_1$ [Fig. 2(c)] reveals a vertical valley at $A = 1$ and a diagonal valley. Juxtaposing the $\phi_{2Q} = 180°$ contour from Fig. 2(b), we observe the matching of PC at the crossing of these valleys, in excellent agreement with a numerical two-qutrit simulation [Fig. 2(d)].

Experimentally, due to the discreteness of t_s, it is unlikely to precisely match $t_p/2$ to the half-pulse duration that truly maximizes $P_{|2\rangle}$. To understand the consequences, we examine the ϕ_{2Q} and $\tilde{L}_1$ landscapes for SNZ pulses upon intentionally changing t_p by $\pm 6t_s$ (Fig. 3). While the PC contour remains roughly unchanged in both cases, there are significant effects on $\tilde{L}_1$. In both cases, we observe that $\tilde{L}_1$ lifts at the prior crossing of LC1 and LC3 valleys where

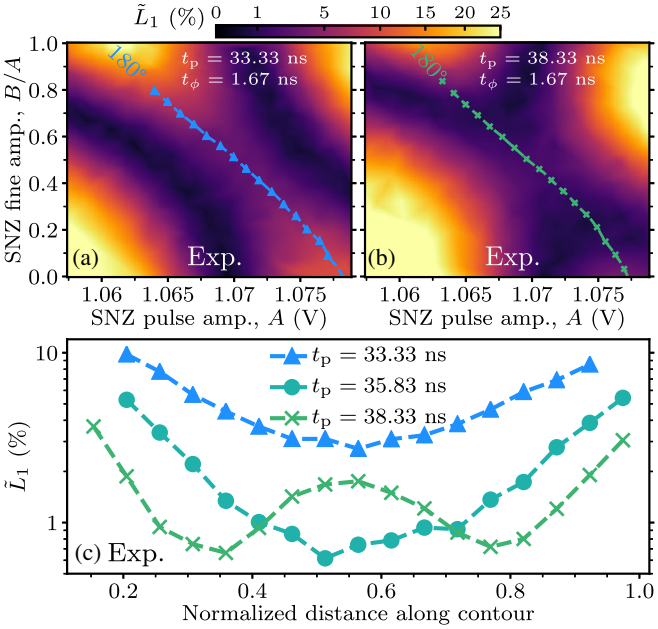

FIG. 3. (a),(b) Landscapes of the leakage estimate $\tilde{L}_1$ for intentionally short and long SNZ half pulses on Q_{M2}. (c) Extracted $\tilde{L}_1$ along the $\phi_{2Q} = 180°$ contours from (a),(b), and Fig. 2(c).

$\phi_{2Q} = 180°$. For too-short pulses [Fig. 3(a)], there remain two valleys of minimal $\tilde{L}_1$, but these are now curved and do not cross $\phi_{2Q} = 180°$. For too-long pulses [Fig. 3(b)], there are also two curved valleys. Crucially, these cross the $\phi_{2Q} = 180°$ contour, and it remains possible to achieve PC and minimize leakage at two (A, B) settings. Extracting $\tilde{L}_1$ along the $\phi_{2Q} = 180°$ contours [Fig. 3(c)] confirms that too-long pulses can achieve the same minimal $\tilde{L}_1$ as when using the nominal t_p. The impossibility to achieve minimal leakage at $\phi_{2Q} = 180°$ for too-short pulses manifests the speed limit set by J_2. In turn, the demonstrated possibility to do so for too-long pulses (even overshooting by several sampling points) proves the viability of the SNZ pulse in practice.

With these insights, we proceed to tune the remaining SNZ CZ gates following similar procedures. We use final weak bipolar pulses of total duration $t_{1Q} = 10$ ns to null the single-qubit phases in the frame of microwave drives. Since our codeword-based control electronics has a 20 ns timing grid, and $40 \text{ ns} < t_{\text{total}} = t_p + t_\phi + t_{1Q} < 60$ ns for all pairs, we allocate 60 ns to every CZ gate. Some pair-specific details must be noted. Owing to the frequency overlap of Q_{M1} and Q_{M2}, implementing CZ between Q_H and Q_{M1} (Q_{M2}) requires a bipolar parking flux pulse on Q_{M2} (Q_{M1}) during the SNZ pulse on Q_H [6,33]. For most pairs, we employ the $|11\rangle$–$|02\rangle$ interaction, which requires the smallest flux amplitude (reducing the impact of dephasing from flux noise) and does not require crossing any other interaction. However, for Q_L-Q_{M1}, we cannot reliably use this interaction as there is a flickering two-level system (TLS) overlapping with the $|0\rangle$–$|1\rangle$ transition in Q_{M1} at this amplitude [37]. For this pair, we therefore employ the $|11\rangle$–$|20\rangle$ interaction. Here, SNZ offers a side benefit: it crosses the Q_{M1}-TLS, $|11\rangle$–$|02\rangle$, and $|01\rangle$–$|10\rangle$ resonances as suddenly as possible, minimizing population exchange.

Table I summarizes the timing parameters and performance attained for the four SNZ CZ gates. The CZ gate fidelity F and leakage L_1 are extracted using a 2QIRB protocol [29,32]. For each pair, we report the average and standard deviation of both based on at least 10 repetitions of the protocol spanning more than 8 h [37]. Several observations can be drawn. First, CZ gates involving Q_H perform better on average than those involving Q_L. This is likely due to the shorter t_{lim} and correspondingly longer time 60 ns $-t_p$ spent near the sweetspot. Additionally, the frequency downshifting required of Q_H to interact with the midfrequency transmons is roughly half that required of the latter to interact with Q_L. This reduces the impact of dephasing from flux noise during the pulse. Not surprisingly, performance is worst for $Q_L - Q_{M1}$. Here, the pulse must downshift Q_{M1} the most to reach the distant $|11\rangle$–$|20\rangle$ interaction, increasing dephasing from flux noise. Also, there may be residual exchange at the crossed resonances. Overall, there is significant temporal variation in performance as gleaned by repeated 2QIRB characterizations. We believe this reflects the underlying variability of qubit relaxation and dephasing times and flux offsets, which, however, were not tracked simultaneously. In addition to having the best average performance, pair Q_{M2}-Q_H displays the maximum F of $99.93 \pm 0.24\%$ (Fig. 4) extracted from a single 2QIRB characterization. To the best of our knowledge, this is the highest CZ fidelity extracted from one 2QIRB characterization in a multitransmon processor.

To understand the dominant sources of infidelity $\varepsilon = 1 - F$ and leakage, we run numerical simulations [29], for both SNZ and CNZ, with experimental input parameters for pair Q_{M2}-Q_H. We dissect an error budget versus various models finding similar contributions for both gates (see Supplemental Material [37]). Nevertheless, the results suggest that SNZ slightly outperforms CNZ, likely due to a shorter time spent away from the sweetspot during the fixed 60 ns allocated for both variants. This confirms that the temporary full transfer from $|11\rangle$ to $|02\rangle$ does not compromise the gate fidelity.

In summary, we have proposed and realized high-fidelity CZ gates using the sudden version of the net zero bipolar fluxing scheme. SNZ CZ gates operate ever closer to the

TABLE I. Summary of SNZ CZ pulse parameters and achieved performance for the four transmon pairs. Single-qubit phase corrections are included in t_{total}. Gate fidelities and leakage are obtained from 2QIRB keeping the other two qubits in $|0\rangle$. Statistics (average and standard deviation) are taken from repeated 2QIRB runs (see Supplemental Material [37] for technical details). The maximum F and minimum L_1 quoted are not necessarily from the same run.

Parameter	Q_{M1}-Q_H	Q_{M2}-Q_H	Q_L-Q_{M1}	Q_L-Q_{M2}
t_{lim} (ns)	31.0	27.6	38.4	33.8
t_p, t_ϕ (ns)	32.50,2.92	29.10,3.75	40.83,1.25	35.83,1.67
t_{total} (ns)	45.42	42.91	52.08	47.50
Interaction	$\|11\rangle$–$\|02\rangle$	$\|11\rangle$–$\|02\rangle$	$\|11\rangle$–$\|20\rangle$	$\|11\rangle$–$\|02\rangle$
Parked qubit	Q_{M2}	Q_{M1}	...	...
Avg. F (%)	98.89 ± 0.35	99.54 ± 0.27	93.72 ± 2.10	97.14 ± 0.72
Avg. L_1 (%)	0.13 ± 0.02	0.18 ± 0.04	0.78 ± 0.32	0.63 ± 0.11
Max. F (%)	99.77 ± 0.23	99.93 ± 0.24	99.15 ± 1.20	98.56 ± 0.70
Min. L_1 (%)	0.07 ± 0.04	0.10 ± 0.02	0.04 ± 0.08	0.41 ± 0.10

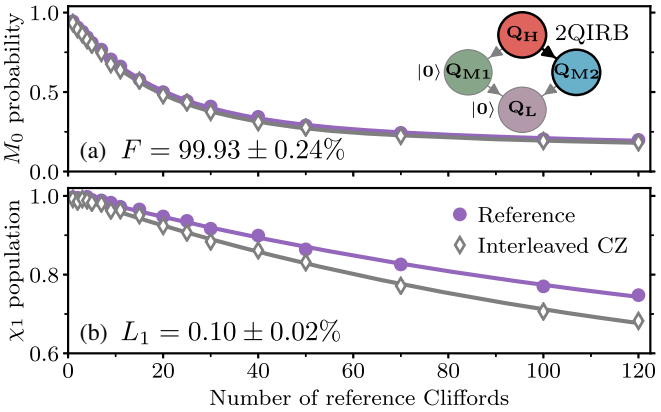

FIG. 4. Best SNZ CZ gate performance achieved from a single run of 2QIRB. (a) Reference and CZ-interleaved return probability M_0 to $|00\rangle$ and (b) population in the computational space χ_1 as a function of the number of two-qubit Cliffords in the reference curve. Errors bars in F and L_1 are obtained from the uncertainty of exponential-decay fits.

speed limit of transverse coupling by maximizing intermediate leakage to the noncomputational state. Control architectures without a timing grid will benefit most from the speedup of SNZ over CNZ by reducing total gate time and thereby minimizing the impact of decoherence. A demonstrated second key advantage of SNZ over CNZ is ease of tuneup, owing to the simple structure of error landscapes as a function of pulse parameters. Harnessing the tuning simplicity, we already employ SNZ CZ gates in the Starmon-5 processor publicly available via the QuTech Quantum Inspire platform [45]. Moving forward, the compatibility of SNZ with our scalable scheme [33] for surface coding makes SNZ our choice for CZ gates for quantum error correction. Finally, the straightforward extension of SNZ to arbitrary conditional-phase gates will find immediate use in NISQ applications.

The data presented in this paper and in its Supplemental Material are available at [46].

We thank L. Janssen, M. Rol, M. Sarsby, T. Stavenga, B. Tarasinski, and M. Venkatesh for experimental assistance, C. Eichler and B. Terhal for discussions, and G. Calusine and W. Oliver for providing the traveling-wave parametric amplifier used in the readout amplification chain. This research is supported by the Office of the Director of National Intelligence (ODNI), Intelligence Advanced Research Projects Activity (IARPA), via the U.S. Army Research Office Grant No. W911NF-16-1-0071, and by Intel Corporation. The views and conclusions contained herein are those of the authors and should not be interpreted as necessarily representing the official policies or endorsements, either expressed or implied, of the ODNI, IARPA, or the U.S. Government. F B. is supported by ERC Grant EQEC No. 682726.

*These authors contributed equally to this work.

[1] M. Kjaergaard, M. E. Schwartz, J. Braumller, P. Krantz, J. I.-J. Wang, S. Gustavsson, and W. D. Oliver, Annu. Rev. Condens. Matter Phys. **11**, 369 (2020).
[2] F. Arute *et al.*, Nature (London) **574**, 505 (2019).
[3] A. G. Fowler, M. Mariantoni, J. M. Martinis, and A. N. Cleland, Phys. Rev. A **86**, 032324 (2012).
[4] C. C. Bultink, T. E. O'Brien, R. Vollmer, N. Muthusubramanian, M. W. Beekman, M. A. Rol, X. Fu, B. Tarasinski, V. Ostroukh, B. Varbanov, A. Bruno, and L. DiCarlo, Sci. Adv. **6**, eaay3050 (2020).
[5] C. K. Andersen, A. Remm, S. Lazar, S. Krinner, J. Heinsoo, J.-C. Besse, M. Gabureac, A. Wallraff, and C. Eichler, npj Quantum Inf. **5**, 69 (2019).
[6] C. K. Andersen, A. Remm, S. Lazar, S. Krinner, N. Lacroix, G. J. Norris, M. Gabureac, C. Eichler, and A. Wallraff, Nat. Phys. **16**, 875 (2020).
[7] F. W. Strauch, P. R. Johnson, A. J. Dragt, C. J. Lobb, J. R. Anderson, and F. C. Wellstood, Phys. Rev. Lett. **91**, 167005 (2003).
[8] L. DiCarlo, J. M. Chow, J. M. Gambetta, L. S. Bishop, B. R. Johnson, D. I. Schuster, J. Majer, A. Blais, L. Frunzio, S. M. Girvin, and R. J. Schoelkopf, Nature (London) **460**, 240 (2009).
[9] S. Sheldon, E. Magesan, J. M. Chow, and J. M. Gambetta, Phys. Rev. A **93**, 060302(R) (2016).
[10] S. S. Hong, A. T. Papageorge, P. Sivarajah, G. Crossman, N. Didier, A. M. Polloreno, E. A. Sete, S. W. Turkowski, M. P. da Silva, and B. R. Johnson, Phys. Rev. A **101**, 012302 (2020).
[11] R. Barends *et al.*, Phys. Rev. Lett. **123**, 210501 (2019).
[12] B. M. Varbanov, F. Battistel, B. M. Tarasinski, V. P. Ostroukh, T. E. O'Brien, L. DiCarlo, and B. M. Terhal, npj Quantum Inf. **6**, 102 (2020).
[13] P. Aliferis and B. M. Terhal, Quantum Inf. Comput. **7**, 139 (2007).
[14] J. Ghosh, A. G. Fowler, J. M. Martinis, and M. R. Geller, Phys. Rev. A **88**, 062329 (2013).
[15] A. G. Fowler, Phys. Rev. A **88**, 042308 (2013).
[16] M. Suchara, A. W. Cross, and J. M. Gambetta, Quantum Inf. Comput. **15**, 997 (2015).
[17] J. Ghosh and A. G. Fowler, Phys. Rev. A **91**, 020302(R) (2015).
[18] L. DiCarlo, M. D. Reed, L. Sun, B. R. Johnson, J. M. Chow, J. M. Gambetta, L. Frunzio, S. M. Girvin, M. H. Devoret, and R. J. Schoelkopf, Nature (London) **467**, 574 (2010).
[19] R. Barends *et al.*, Nature (London) **508**, 500 (2014).
[20] J. Kelly *et al.*, Nature (London) **519**, 66 (2015).
[21] J. M. Martinis and M. R. Geller, Phys. Rev. A **90**, 022307 (2014).
[22] S. Krinner, S. Lazar, A. Remm, C. K. Andersen, N. Lacroix, G. J. Norris, C. Hellings, M. Gabureac, C. Eichler, and A. Wallraff, Phys. Rev. Applied **14**, 024042 (2020).
[23] Y. Chen *et al.*, Phys. Rev. Lett. **113**, 220502 (2014).
[24] F. Yan, P. Krantz, Y. Sung, M. Kjaergaard, D. L. Campbell, T. P. Orlando, S. Gustavsson, and W. D. Oliver, Phys. Rev. Applied **10**, 054062 (2018).
[25] P. Mundada, G. Zhang, T. Hazard, and A. Houck, Phys. Rev. Applied **12**, 054023 (2019).

[26] M. C. Collodo, J. Herrmann, N. Lacroix, C. K. Andersen, A. Remm, S. Lazar, J.-C. Besse, T. Walter, A. Wallraff, and C. Eichler, Phys. Rev. Lett. **125**, 240502 (2020).
[27] Y. Xu, J. Chu, J. Yuan, J. Qiu, Y. Zhou, L. Zhang, X. Tan, Y. Yu, S. Liu, J. Li, F. Yan, and D. Yu, Phys. Rev. Lett. **125**, 240503 (2020).
[28] J. A. Schreier, A. A. Houck, J. Koch, D. I. Schuster, B. R. Johnson, J. M. Chow, J. M. Gambetta, J. Majer, L. Frunzio, M. H. Devoret, S. M. Girvin, and R. J. Schoelkopf, Phys. Rev. B **77**, 180502(R) (2008).
[29] M. A. Rol, F. Battistel, F. K. Malinowski, C. C. Bultink, B. M. Tarasinski, R. Vollmer, N. Haider, N. Muthusubramanian, A. Bruno, B. M. Terhal, and L. DiCarlo, Phys. Rev. Lett. **123**, 120502 (2019).
[30] M. Kjaergaard *et al.*, arXiv:2001.08838.
[31] E. Magesan, J. M. Gambetta, and J. Emerson, Phys. Rev. A **85**, 042311 (2012).
[32] C. J. Wood and J. M. Gambetta, Phys. Rev. A **97**, 032306 (2018).
[33] R. Versluis, S. Poletto, N. Khammassi, B. M. Tarasinski, N. Haider, D. J. Michalak, A. Bruno, K. Bertels, and L. DiCarlo, Phys. Rev. Applied **8**, 034021 (2017).
[34] N. Lacroix, C. Hellings, C. K. Andersen, A. Di Paolo, A. Remm, S. Lazar, S. Krinner, G. J. Norris, M. Gabureac, J. Heinsoo, A. Blais, C. Eichler, and A. Wallraff, PRX Quantum **1**, 110304 (2020).
[35] R. Barends *et al.*, Nat. Commun. **6**, 7654 (2015).
[36] J. Preskill, Quantum **2**, 79 (2018).
[37] See Supplemental Material at http://link.aps.org/supplemental/10.1103/PhysRevLett.126.220502 for additional information supporting statements and claims made in the main text, which includes Refs. [4,21,29,38–43].
[38] J. Heinsoo, C. K. Andersen, A. Remm, S. Krinner, T. Walter, Y. Salathé, S. Gasparinetti, J.-C. Besse, A. Potočnik, A. Wallraff, and C. Eichler, Phys. Rev. Applied **10**, 034040 (2018).
[39] B. Nijholt, J. Weston, J. Hoofwijk, and A. Akhmerov, Adaptive: Parallel Active Learning of Mathematical Functions (Zenedo, 2019), https://doi.org/10.5281/zenodo.1182437.
[40] P. Krantz, M. Kjaergaard, F. Yan, T. P. Orlando, S. Gustavsson, and W. D. Oliver, Appl. Phys. Rev. **6**, 021318 (2019).
[41] C. C. Bultink, B. Tarasinski, N. Haandbaek, S. Poletto, N. Haider, D. J. Michalak, A. Bruno, and L. DiCarlo, Appl. Phys. Lett. **112**, 092601 (2018).
[42] F. Motzoi, J. M. Gambetta, P. Rebentrost, and F. K. Wilhelm, Phys. Rev. Lett. **103**, 110501 (2009).
[43] J. M. Chow, L. DiCarlo, J. M. Gambetta, F. Motzoi, L. Frunzio, S. M. Girvin, and R. J. Schoelkopf, Phys. Rev. A **82**, 040305(R) (2010).
[44] M. A. Rol, L. Ciorciaro, F. K. Malinowski, B. M. Tarasinski, R. E. Sagastizabal, C. C. Bultink, Y. Salathe, N. Haandbaek, J. Sedivy, and L. DiCarlo, Appl. Phys. Lett. **116**, 054001 (2020).
[45] QuTech Quantum Inspire, https://www.quantum-inspire.com/.
[46] https://github.com/DiCarloLab-Delft/High_Fidelity_ControlledZ_Data/.